# *n*-Alkane-based reconstructions of peat accumulations and depositional conditions at four locations around a shallow maar lake in the Changbai Mountains, northeastern China

Yan Zhang[a], Chuanyu Gao[b], Shaoqing Zhang[b], Ping Yang[a], Philip A. Meyers[c]*, Guoping Wang[b,]*

[a] *Key Laboratory of Humid Subtropical Eco-Geographical Process, Ministry of Education, Institute of Geographical Sciences, Fujian Normal University, Fuzhou, 350007, China*

[b] *Key Laboratory of Wetland Ecology and Environment, Northeast Institute of Geography and Agroecology, Chinese Academy of Sciences, Changchun, 130102, China*

[c] *Department of Earth and Environmental Sciences, The University of Michigan, Ann Arbor, Michigan, 48109-1005, USA*

* Corresponding authors.
Philip A Meyers, pameyers@umich.edu, Tel: +1-734-330-3873, ORCID 0000-0002-9709-7528
Guoping Wang, wangguoping@iga.ac.cn, Tel: +86-0431-85542339

Key points:

- *n*-Alkane-based reconstruction of peat accumulation history around a maar lake.
- Hydrological conditions and plant communities related to lake basin caused by volcanism lead to unsynchronized peat depositional processes.
- Volcanism and anthropogenic have important impacts on local peat development.

**Abstract**

A high-resolution *n*-alkane biomarker study of peat cores from four locations around the Yuanchi maar lake in the Changbai Mountains of northeastern China, has revealed different histories of peat deposition in the closely located sequences, although they experienced the same paleoclimate changes. Comparisons of the *n*-alkane distributions of modern plants around the lake and those in the peat cores suggest that the disparate peat development patterns in the four sites are the consequence of different peat-forming communities growing around the lake. These floral differences were in turn controlled by different water depths associated closely with the volcanogenic lava- and tephra-shaped topography of the lake basin. Moreover, the *n*-alkane-inferred variations in peat development patterns and inferred recent climate changes around Yuanchi Lake relate closely to the histories of volcanic forcing in the tropical Pacific and local volcanic eruptions of the Changbai Mountains. These events evidently led to alterations of local climate that affected growth of land plants at the four locations. Finally, anthropogenic impacts since 1950 CE have had an additional effect on peat accumulation in the Changbai Mountains region.

**Keywords:** peat deposition, *n*-alkanes, local conditions, volcanic eruption, anthropogenic activities, Changbai Mountains

## 1. Introduction

Peat is the partially preserved remains of former plant communities that contains a high proportion of organic matter (OM). Peatlands therefore can be either sources or sinks of carbon depending on environmental conditions (Kayranli et al., 2010; Naafs, et al., 2019). Different types of peatlands are defined by their distinctive combinations of hydrology and chemistry that support characteristic plant communities (Andersson et al., 2012). Lipid biomarkers have special features of relative source specificity and resistance to decomposition. The composition and abundance of biomarkers in peat are mainly derived from waxes of plants that grew where the peat accumulated (e.g. Nichols et al., 2006; Zheng et al., 2007; Zhou et al., 2005; Andersson et al., 2011; Zhang et al., 2014, 2016, 2017). Lipid biomarkers in continuous peat cores consequently can provide information on variations in former plant communities that contributed to peat deposition and provide site-specific records of *in situ* environmental histories (e.g. Regnery et al., 2013; Zhang et al., 2018; Naafs et al., 2019).

Peatlands are widely distributed in northeast China. Many studies have focused on them to provide detailed paleoenvironmental reconstructions on centennial and millennial age-scales (e.g. Hong et al., 2001; Zhou et al., 2005; Zhang et al., 2015, 2016; Zhang et al., 2014, 2017). The Changbai Mountains in northeastern China are comprised of a group of volcanoes. Most peatlands in these mountains have developed in lava-dammed lakes or shallow crater lakes, and apparent differences in the initial time and development of peat deposition exist between the two types of volcanogenic landforms (Yang, 1995; Xing et al., 2019). Unlike the Jinchuan and Hani peatlands that

68 evolved from lava-dammed lakes and began to accumulate before 10 ka, more recent
69 peatlands such as the Yuanchi and Chichi peatlands developed from maar lakes that
70 formed in shallow and irregular depressions resulting from inactive volcanic craters.
71 Therefore, both the accumulation time and the thickness of the peat deposited in those
72 regions are smaller than those in the peatlands that evolved from lava-dammed lakes
73 (Yang et al., 1995). To date, studies of the longer-lived peatlands have yielded valuable
74 information about the long-term regional climate changes (e.g. Hong et al., 2001; Seki et
75 al., 2009; Zhou et al., 2010). However, little is known about modern peat deposition
76 process and its possible controlling factors in the peatlands that derived from the shallow
77 crater lakes in the Changbai Mountains.

78 Even small volcanic eruptions commonly inject large quantities of aerosols and ash
79 into the atmosphere that alter the radiative balance and chemical equilibrium of the
80 stratosphere, thereby impacting regional climate (Xu et al., 2012; Sun et al., 2014, 2015).
81 A Plinian eruption in the Changbai Mountains around 1000 years ago (the Millennium
82 Eruption), which was accompanied by an earthquake with a magnitude of ~7, was one of
83 the most violent eruptions in history (Sun et al., 2014, 2015). Hereafter, three
84 small-scale volcanic eruptions, in 1668 CE, 1702 CE, and 1903 CE, also documented in
85 the Mountains (Xu et al., 2012). In addition, population growth and economic
86 development around the Changbai Mountains area in recent years also have had a
87 significant impact on local conditions (Gao et al., 2016; Bao et al., 2019). These
88 volcanism and anthropogenic impacts on local conditions consequently could have had
89 important impacts on plant growth that directly affected peat accumulations. However,

scant information is available about details of the peat deposition process and its potential responses to volcanic or anthropogenic activities in this region.

We present here a well-resolved record of the amounts and distributions of *n*-alkane biomarkers in modern plant communities and associated peat cores from four different sites around a modern peatland that evolved from a shallow maar lake (Yuanchi Lake) in the Changbai Mountains. The main objectives of this study are (1) to reconstruct a decade-scale history of peat-forming communities that influenced peat deposition around the maar lake, (2) to understand the localized responses of peat depositional processes to variations in plant assemblages and local conditions caused by volcanic eruptions, and (3) to explore the influences of volcanism and modern anthropogenic impacts on peat deposition in this region.

## 2. Materials and methods

### *2.1 Study area*

The Changbai Mountains are in the Jilin Province of northeastern China and extend along the boundary between China and North Korea. The area has a continental monsoon climate with long, cold winters and short, cool summers. More detailed descriptions on the regional character have been described by Bao et al. (2010) and Gao et al. (2016). Many lakes that formed from volcanic dams and in volcanic craters exist in this region. Both the climate conditions and the topographic features in the region result in extensive development of peatlands from lava-dammed lakes or shallow crater lakes (Chai, 1990).

Yuanchi Lake (42º01'52"~42º01'58" N，128º26'03"~128º26'10" E; elevation ca. 1280

112 m asl) has a diameter of 180 m and a catchment area of 4.1 $hm^2$, located on the eastern
113 slopes and about 30 km from the main peak of the Changbai Mountains (Figs.1 and 2). It
114 partially fills a volcanic crater and has no significant inflow or outflow from surface
115 water or groundwater (Yang, 1995; Bao et al., 2010). Peatlands are distributed around
116 the perimeter of the lake and are populated by different peat-forming plant communities
117 (Fig.2). The modern biomes in the surroundings of the lake are trees and shrubs,
118 including *L. olgensis, B. fruticosa, V.uliginosum, R.parvifolium* and *L. palustre*. The
119 plant community on the west side of YC lake ($YC_W$) is dominated by *C. lasiocarpa* and
120 *Sphagnum* spp, and some *P. australis* and *S. triqueter* grow near the lake shore. On the
121 south edge of lake ($YC_S$), the peat-forming plants are dominated by *C. lasiocarpa*， and
122 extensive developments of emersed vascular plants (*T. orientalis* and *P. australis*) are in
123 this location. On the east side of the lake ($YC_E$), the peat-forming plants are dominated
124 by shrubs, including *V. uliginosum, R. parvifolium,* and *L. palustre,* and some *Sphagnum*
125 mounds are distributed among the shrubs. The north side of the lake ($YC_N$) is dominated
126 by *Sphagnum* spp. Large amounts of shrubs (*V. uliginosum* and *Rhododendron*
127 *parvifolium*) mixed with *L. olgensi, B. fruticosa and Lonicera caerulea* also appear in
128 this location.

129 *2.2. Sample collection and stratigraphy*

130 Four peat-mud cores were collected around the edges of Yuanchi Lake ($YC_E$, $YC_W$,
131 $YC_S$ and $YC_N$) with a Wardenaar peat sampler in September, 2006. The lithologies of
132 each core show that the cores contain distinctive stratigraphic sequences based on
133 texture, peat color, plant remains, and TOC contents (Fig.3). For $YC_W$, the top 8 cm

consists of brown peat having a small amount of partially decomposed *Carex* remains, then a layer from 8 cm to 29 cm containing dark brown peat with a high degree of decomposition, and finally black mud underlying the peat sequence. In the YCs core, the peat layer in the top 13 cm is composed of brown peat, the interval from 13 cm to 28 cm is dark brown peat, and black mud occupies the bottom of the core. For $YC_E$, the brown peat layer comprises the top 8 cm, dark brown peat with higher degree of decomposition occupies the interval from 7 to 35 cm, and black mud is present below 35 cm. In the $YC_N$ core, a brown moss-peat layer dominated by *Sphagnum* spp. constitutes the top 14 cm, then a brown peat layer occupies the interval from 14 to 21 cm, the interval from 21 cm to 28 cm is dark brown peat with a high degree of decomposition, then the black mud occupies the bottom of the core. The cores were subsampled on-site by slicing into 1 cm intervals that were stored in polyethylene bags for transport to the laboratory for analysis.

### *2.3. Chronology of the peat-mud sequence*

The peat cores were dated at 1 cm intervals by $^{210}$Pb analysis. A collective total of 120 peat samples from the four cores were analyzed using a low-background γ-ray spectrometer with a high-purity Ge semiconductor (ORTEC Instruments Ltd., USA) at the State Key Laboratory of Lake Science and Environment, Nanjing Institute of Geography and Limnology, CAS. The radioisotope results and the age-depth model were described in more detail by Bao et al. (2010). Peat accumulation rates (PAR, cm/yr) were estimated from the 1 cm depth intervals and the corresponding $^{210}$Pb ages.

### *2.4. Laboratory analysis*

156 The peat samples taken at 1 cm intervals from the peat cores were dried at 105 °C and
157 then combusted in a muffle furnace at 550 °C for 4h to determine their loss on ignition
158 (LOI) values (Heiri et al., 2001). TOC concentration of each sample was estimated from
159 OM content expressed as LOI values by multiplying the LOI by 0.5, and organic carbon
160 accumulation rates (CAR, g C/m$^2$/yr)) were calculated from the TOC concentrations and
161 the PAR values (Bao et al., 2010).

162 For *n*-alkane analyses, air-dried samples (1g) were extracted three times with
163 MeOH/dichloromethane (1:1, v:v) for 15 min in an accelerated solvent extractor. The
164 three extracts were combined after filtration and concentrated using a rotary evaporator.
165 The *n*-alkanes were isolated using silica gel column chromatography by elution with 20
166 ml *n*-hexane. The eluate was concentrated with a $N_2$ stream and transferred to vials for
167 gas chromatography-mass spectrometry (GC-MS) analysis. Details of the *n*-alkane
168 analysis and determination are described by Zhang et al. (2014, 2016).

169 *2.5 n-Alkane proxies*

170 We employ a suit of *n*-alkane molecular ratios as proxies to identify changes in the
171 origins of the biomarker molecules and in their relative amounts of preservation, two
172 parameters that are commonly sensitive to climate changes. These ratios include the
173 total *n*-alkane concentrations normalized to TOC (μg total *n*-alkanes/g TOC), carbon
174 preference index (CPI), average chain length (ACL), and the proportion of aquatic
175 components ($P_{aq}$). These derived ratios collectively summarize variations of *n*-alkane
176 distributions in the peat sequences (e.g. Naafs et al., 2019. The *n*-alkane CPI values
177 reflecting the odd-over-even predominance of the carbon-chain-length have been

interpreted as an indicator of extensive microbial degradation of *n*-alkanes in peat sequences (Zhou et al., 2010). The *n*-alkane ACL describes the weighted mean lipid chain length and reflects the dominant chain-lengths of the *n*-alkanes. We calculated the CPI and ACL values over the carbon atom range of 20-33. The $P_{aq}$ was defined using lacustrine vegetation (Ficken et al., 2000), but it is also used to reconstruct the proportions of aquatic plants or mosses in peat, which is a parameter that indicates peat hydrological conditions (e.g, Zhou et al., 2005, Nichols et al., 2006; Zhang et al., 2016, 2017).

## 3. Results

### *3.1 The age-depth chronologies, TOC concentrations and PARs of the four peat sequences*

The $YC_w$ age-depth scale indicates that the 29-cm thick peat layer in this sequence was deposited during the past ca. 400 years, from 1600 to 2000 CE (Fig.3a). The TOC concentration ranges from 19.5 to 48.2%, with a mean value of 40.3±8.5%. Continuous increases in TOC concentrations occur in the bottom of the peat core, and notably high and stable values (mean 44.6±2.9%) appear in the upper 20-cm section that corresponds to peat deposition since 1800 CE (Fig.3b). PAR varies from 0.03 to 0.33 cm/yr in the $YC_w$ sequence (Fig.3b). The rate is initially very slow (~0.04 cm/yr) and increases slightly to 0.1 cm/yr in the interval from 20 to 13 cm (from 1800 to 1900 CE). Then the rates increase markedly and peak at 8 cm (ca.1950 CE).

The peat in the upper 28 cm of the YCs sequence was deposited during the last 200 years, from 1800 to 2000 CE (Fig.3c). TOC concentrations range from 3.4 to 39.5 %,

200 with a mean value of 28.8±10.5%. Relatively higher TOC values (mean 31.6±7.0%)
201 occur in the top 25 cm, corresponding to deposition since 1850 CE (Fig.3d). PAR ranges
202 between 0.04 and 0.33 cm/yr in the $YC_s$ peat section (Fig.3d). Lower rates less than 0.1
203 cm/yr occur below 25 cm, then the rate increases gradually to a maximum (0.33 cm/yr)
204 at 8 cm (ca. 1950 CE) before decreasing sharply to ~0.1 cm/yr in the top 5 cm of the
205 core.

206 The age-depth scale of the $YC_E$ sequence indicates that the peat in the top 35 cm was
207 deposited during the past ca. 400 years, from 1600 to 2000 CE (Fig.3e). The TOC
208 concentrations in the peat vary between 10.7 and 51.1%, with a mean value of
209 33.6±8.3%. High values (>30%) and a gradually increasing trend starting at 28 cm
210 correspond to accumulation since 1800 CE (Fig.3f). The PAR in the $YC_E$ peat section
211 fluctuates between 0.04 and 0.59 cm/yr (Fig.3f). Markedly lower values occur below 28
212 cm (before 1800 CE), then the rates start to increase slightly but fluctuate strongly, and
213 relatively higher values appear in the upper 8 cm (since 1950 CE).

214 The $YC_N$ peat layer was deposited during the past ca. 250 years, from 1750 to 2000
215 CE (Fig.3g). The TOC concentrations range from 13.1 to 51.4% (mean 38.4±11.5%),
216 with obviously high and ever-increasing values (mean 43.2±6.5%) in the upper 25 cm
217 that corresponds to peat deposition since 1800 CE (Fig.3h). The PAR has lower values at
218 the bottom of this peat section below 25 cm, and higher values occur from 22 to 19 cm.
219 Markedly lower values (~0.08 cm/yr) appear again from 19 to 10 cm (1850 to 1950 CE)
220 before increasing markedly in the top 10 cm (since 1950 CE) (Fig.3h).

221 *3.2. n-Alkane distributions*

222 The *n*-alkane distributions from the different layers in the four peat sequences range
223 similarly from $C_{20}$ to $C_{33}$ and have an odd/even predominance with a dominance of
224 middle and long chain components (Fig.4). The *n*-alkane distributions in the whole $YC_w$
225 peat core have a strong dominance of the $C_{27}$ component, and *n*-$C_{23}$ also contributes
226 high proportions in the upper and bottom peat units**.** The $YC_s$ peat core is characterized
227 by strong dominances of $C_{23}$, $C_{25}$ and $C_{27}$ *n*-alkanes in different peat layers. For the $YC_E$
228 peat core, the distribution in the brown peat unit is dominated by the $C_{23}$ and $C_{31}$
229 *n*-alkanes and in the dark brown peat by the $C_{27}$ and $C_{31}$ *n*-alkanes. In the $YC_N$ peat core,
230 long-chain $C_{29}$ and $C_{31}$ *n*-alkanes are the major components in the upper unit and the
231 bottom of the core, and the middle brown moss peat layer has abundant middle chain $C_{23}$
232 and $C_{25}$ in subequal proportions with the long chain *n*-alkanes.

233 *3.3. n-Alkane concentrations and their molecular ratios*

234 We focus on *n*-alkane-based reconstruction of the peat deposition history and
235 paleoenvironmental information in the Yuanchi Lake region. Here we present the results
236 of the changes in TOC concentrations, the PARs, the CARs, and the *n*-alkane
237 concentrations and their derived molecular climate proxies (CPI, ACL and $P_{aq}$) for the
238 four peat sequences that we collected around Yuanchi Lake (Figs.5-8).

239 The total *n*-alkane concentrations normalized to TOC in the $YC_W$ core range between
240 42.2 and 595.7 μg/g TOC, with a mean value of 188.5±176.3 μg/g. Markedly higher
241 values occur before 1800 CE and lower values appear from 1800 CE to present (Fig.5c).
242 The *n*-alkane CPI varies between 2.1 and 4.2, with a mean value of 3.2±0.5 (Fig.5d).
243 ACL and $P_{aq}$ values range from 24.3 to 26.4 (mean 25.6±0.5) and 0.5 to 0.9 (mean

244 0.7±0.09), respectively (Fig.5e and f). Gradually increasing CPIs exist before 1800 CE,
245 and lower ACL but higher $P_{aq}$ values occur in this interval. Markedly decreasing CPIs,
246 higher ACL but lower $P_{aq}$ values appear from 1800 to 1900 CE, corresponding to the
247 highest TOC concentrations (Fig.5a). The interval from 1940 to present is characterized
248 by the lowest CPI and ACL values and the highest $P_{aq}$ value, coinciding with the higher
249 TOC concentrations and higher PAR and CAR values (Fig.5a and b).

250 In the $YC_S$ sequence, the total *n*-alkane concentrations range between 56.6 and 529.4
251 μg/g TOC, with a mean value of 226.1±134.6 μg/g (Fig.6c). Relatively higher
252 concentrations appear before 1850 CE, and the values decrease sharply to the minimum
253 at ca. 1900 CE. Then higher values appear again in the interval between 1900 and 1950
254 CE, and stably lower values occur from 1950 CE to the present. This variation generally
255 corresponds to the PAR changes in those time (Fig.6 and c). The *n*-alkane CPIs vary
256 between 2.6 and 4.9 (mean 3.5±0.6), and ACLs vary between 24.5 and 26 (mean
257 25.4±0.5), and the $P_{aq}$ values change inversely to the ACL values, ranging from 0.6 to
258 0.85 (mean 0.7±0.07) (Fig.6d-f). Markedly lower ACLs (<25) but higher $P_{aq}$ values
259 (>0.7) appear before 1850 CE and during the interval between 1900 and 1950 CE,
260 corresponding to the relatively higher PAR, CAR and total *n*-alkane concentrations in
261 these times (Fig.6b and c).

262 In the $YC_E$ sequence, the total *n*-alkane concentrations range from 3.0 to 482.8 μg/g
263 TOC, with a mean value of 83.8±103.4 μg/g (Fig.7c). The concentrations are generally
264 higher (~120 μg/g) before 1900 CE, but the values are almost below 50 μg/g TOC from
265 1900 to the present. The *n*-alkane CPIs vary widely between 1.3 and 10.7 (mean

266 3.8±1.9), and most of them are lower than 4.0 before 1950 CE, except for the relatively
267 higher values at ca. 1825 CE and 1900 CE, and in the interval from 1950 to the present
268 (Fig.7d). ACLs and $P_{aq}$ values fluctuate between 24.4 and 28.3 (mean 26.2±1.0), and 0.3
269 and 1.0 (mean 0.5±0.2), respectively (Fig.7e and f). Relatively higher ACLs (>26) but
270 lower $P_{aq}$ values (<0.4) appear before 1800 CE, and lower ACLs but higher $P_{aq}$ values
271 occur during the intervals from 1800 to 1950 CE. The ACLs then increase dramatically,
272 in contrast to CPIs and $P_{aq}$ values that decrease markedly during the recent decades
273 (Fig.7d-f), coinciding with the highest TOC, PAR and CAR values but with the lowest
274 *n*-alkane concentrations (Fig.5a-c).

275 The total *n*-alkane concentrations in the $YC_N$ sequence range from 3.7 to 570 μg/g
276 TOC, with a mean value of 172.4±182.8 μg/g (Fig.8c). Markedly higher concentrations
277 (~400 μg/g TOC) appear before 1850 CE, accompanied with higher PARs but lower
278 CARs (Fig.8b); then the values decrease rapidly and most of them below 100 μg/g TOC
279 during the interval from 1850 CE to the present. The *n*-alkane CPIs vary between 1.8
280 and 5.5 (mean 4.0±0.9), with relatively high and stable values (mean 4.4±0.7) before
281 1900 CE (Fig.8d). ACL and $P_{aq}$ values fluctuate between 26.3 and 29.7 (mean 27.8±1.0),
282 and between 0.17 and 0.5 (mean 0.3±0.1), respectively (Fig.8e and f). The highest ACL
283 and the lowest $P_{aq}$ values appear before 1800 CE, and relatively lower ACLs (< 27) but
284 higher $P_{aq}$ values (> 0.4) occur during the intervals from 1800 to 1900 CE; Then
285 markedly higher ACLs (>27.5) but lower $P_{aq}$ values (<0.3) appear again from 1900 CE,
286 which correspond with gradual increases in both CARs and PARs (Fig.8b).

## 4. Discussion

### *4.1 Peat TOC concentrations and peat accumulation processes around the Yuanchi Lake*

Yuanchi Lake is in a circular shallow crater that was formed ca. 1060±100 a B.P (Yang et al., 1995) and was likely related to the Millennium Eruption. The peat layers were deposited in the basin of the maar lake over sediments that are represented by the basal black muds in the four cores (Fig.3). The peat sequences provide records of the succession of peat-forming vegetation that has partially filled the maar lake and evidence of conditions important to the production and preservation of the plant remains (Fig.3). Peat OM is mainly derived from the remains of local plants and provides information about the kinds and amounts of vegetation that has lived in a specific location and the processes that affect peat preservation (Chai, 1990; Meyers and Ishiwatari, 1993; Meyers, 2003; Zhang et al, 2016, 2017). Yuanchi Lake has been filled by ingrowth of peatlands around its edges that have been spreading gradually toward the center of the lake (Yang et al., 1995). The peat $^{210}$Pb-based age-depth models of the four sequences around Yuanchi Lake indicate the initial contributions of TOC-rich vascular plants inputs in the four sites are asynchronous (Fig.3). We hypothesize that this process of transformation of a shallow lake into a peatland first started in the $YC_w$ and $YC_E$ locations ca. 1600 CE, followed by the $YC_N$ ca.1750 CE, with the $YC_s$ starting to infill last since ca.1800 CE (Fig.3).

Although the total histories of peat sequences differ at the four sites, their initiation times for abundant peat accumulations are similar as indicated by the collectively increasing PAR values at ca. 1800 CE (Fig.3). TOC concentrations and PARs in the four

peat sections exhibit increasing trends from 1800 to 1950 CE, suggesting a continuous and growing input of TOC-rich vascular plants promoted peat accumulation around Yuanchi Lake. However, we observe that the mean TOC concentration (~44.6%) in the $YC_w$ peat sequence is higher than in the other three locations (mean 28.8% at $YC_s$, 36% at $YC_E$, and 39% at $YC_N$) since 1800 CE. Nevertheless, mean PAR in the $YC_w$ peat sequence is slightly lower (~0.12 cm/yr) than those values in the other three cores (mean 0.17 cm/yr in $YC_s$, 0.22 cm/yr in $YC_E$, and 0.17 cm/yr in $YC_N$ peat cores) (Fig.3). In addition, differences in peat accumulation between the four locations is evident since 1950 CE, when marked decreases in PAR values occurred in the $YC_w$ and $YC_s$ locations, and the rates in the $YC_E$ and $YC_N$ peat sequences showed rapidly increasing PARs during recent decades (Fig.3). We also observe that the four different locations around Yuanchi Lake are dominated by different vegetation communities (Fig.2), representing settings with different water depths that are likely responsible for the asynchronous peat accumulations. Except for *C. lasiocarpa*, the modern vegetation communities in the $YC_w$ and $YC_s$ sites are dominated by emersed aquatic vascular plants (*T. orientalis* and *P. australis*) that could contribute to higher OM inputs but would be less likely to increase peat accumulate in recent decades as the water became shallower. Moreover, modern vegetation communities at the $YC_E$ and $YC_N$ sites are dominated by *Sphagnum* spp and shrubs growing in shallow water depths that are more likely to promote peat accumulation than *Carex* and the emersed aquatic vascular plants that dominate the $YC_w$ and $YC_s$ sites in deeper-water conditions (Figs.2 and 3).

*4.2. Biomarker distributions in the Yuanchi peat sequences*

331 *4.2.1. n-Alkane biomarkers of modern plants around Yuanchi Lake*

332 *n*-Alkane biomarkers in peat originate mainly from plant waxes and bacteria and are
333 recognized as important proxies for indicating changes in the plant communities and
334 reflecting any alterations from *in situ* processes that peat deposits may experience after
335 their formation (Zhang et al., 2018). The *n*-alkane distribution patterns vary considerably
336 among different peat-forming plant species, a feature that provides important evidence
337 of the main sources of these biomarkers in the peat (e.g. Kirkels et al., 2013; Zhang et al.,
338 2016, 2017). The dominant plants observed at the four sites around Yuanchi lake are
339 clearly different (Fig.2). We compiled published information about the dominant
340 *n*-alkane homologues found in modern plant species like those around the lake to
341 interpret the main sources of the *n*-alkanes in the peat and thereby to provide a
342 biomarker record for reconstructing the *in situ* conditions at the four sites (Table 1).

343 The modern plants in the $YC_W$ site are dominated by *C. lasiocarpa*, *S. triqueter*, and *P.*
344 *australis*, all of which have a predominance of *n*-$C_{29}$ in their *n*-alkane distributions
345 (Cranwell et al.,1984; Street et al., 2013; Ronkainen et al., 2013). Some *Sphagnum* spp
346 characterized by prominent abundances of $C_{23}$ and $C_{25}$ *n*-alkanes (Cranwell et al.,1984;
347 Street et al., 2013) also develop in this site. The *C. lasiocarpa* and *E. fauriei*, which are
348 respectively dominated by *n*-$C_{29}$ and *n*-$C_{27}$ (Tarasov et al., 2013; Ronkainen et al., 2013),
349 are the major modern species growing at the $YC_S$ site. In addition, abundant emersed
350 aquatic vascular plants (*T. orientalis* and *P. australis*), both having a predominance of
351 *n*-$C_{29}$, and some submerged aquatic plants with prominent abundances of $C_{23}$ and $C_{25}$
352 *n*-alkanes (Cranwell et al., 1984; Ficken et al., 2000) are also prevalent in this site under

353 deeper water conditions. The modern vegetation covering both the $YC_E$ and $YC_N$ sites is
354 mainly dominated by *Sphagnum* spp and shrubs (*V. uliginosum* and *R. parvifolium*)
355 under drier condition that are characterized by *n*-$C_{29}$ and *n*-$C_{31}$ (Salasoo, 1987; Tarasov
356 et al., 2013; Street et al., 2013). Moreover, the two sites are surrounded by trees (*L.*
357 *olgensi, B. fruticosa and L. caerulea* ) that have a major predominance of the $C_{27}$
358 *n*-alkane (Tarasov et al., 2013).

359 *4.2.2 Biomarker origins in each of the peat cores from Yuanchi Lake*

360 The chain-length distributions of *n*-alkanes in the four peat sequences range from
361 $C_{20}$ to $C_{33}$ with an odd/even predominance (Fig.3), indicating a major input from
362 terrigenous plant waxes (Eglinton et al., 1967). The dominant *n*-alkane components have
363 different distributions among the four sequences, which can be attributed to origins from
364 different plant types associated with different water levels in their growth locations.
365 Based on the dominant *n*-alkane homologues found in the modern plant covering on the
366 four sites (Table 1), we can infer probable origins of the biomarkers in each of the peat
367 cores (Fig.4).

368 The strong dominance of *n*-alkane $C_{23}$, $C_{25}$ and $C_{27}$ components in the bottom peat
369 units in the $YC_w$ peat core mainly originated from a combination of aquatic plants in a
370 deeper water lake setting and trees from surrounding area. Shallower water along the
371 western edge of the lake and larger amounts of terrestrial plant contributions resulted in
372 the strong dominance of long-chain *n*-alkane in the middle section of the peat core
373 (Fig.4). The abundances of $C_{23}$ and $C_{25}$ components that occur in the upper section is
374 likely associated with increased amounts of *Sphagnum* spp input in recent years. A

375 strong dominance of $C_{23}$, $C_{25}$ and $C_{27}$ *n*-alkanes in the $YC_s$ peat core relate to major
376 contributions from both aquatic plants under high water level condition and terrestrial
377 plants around the area. The *n*-alkane distributions in the $YC_E$ and $YC_N$ peat cores have
378 the long-chain $C_{29}$ and $C_{31}$ *n*-alkanes that are diagnostic of shrub communities in these
379 peat sites (Table 1). In addition, significant proportions of $C_{23}$ and $C_{25}$ *n*-alkanes in the
380 middle and upper sections of the two peat cores suggest important contributions from
381 *Sphagnum* spp, which is consistent with modern plant coverage on the two sites (Fig.2).
382 *4.2.3 Changes in plant communities and site-specific conditions around Yuanchi Lake*
383 The *n*-alkane-based reconstruction of peat deposition in the four settings reveals
384 differences in the rates and composition of peat deposited around Yuanchi Lake (Figs.
385 5-8). In the $YC_w$ site, inputs of vascular plant residues to the paleolake sediments
386 beginning around 1600 CE initiated accumulations of TOC and elevated *n*-alkane
387 concentrations (Fig.5 a and c). The plant communities that developed in this location
388 before 1800 CE were probably dominated by abundant aquatic plants that are typified by
389 short and middle chain lipids (Fig.5e and f). Terrigenous vascular plants characterized
390 by TOC-rich and long-chain lipids began to dominate since 1800 CE, as indicated by the
391 highest TOC concentrations, higher ACL and lower $P_{aq}$ values from 1800 to 1900 CE
392 (Fig.5 a, e and f). These features imply that the relative water depth at this site dropped
393 quickly from 1600 CE as this lakeshore location filled in starting ca. 1800 CE, leading to
394 greater expansion of subaerial TOC-rich vascular plants that promoted peat
395 accumulation. The peat entered a rapid accumulation interval since 1940 CE as evident
396 from the increases in the TOC concentrations and peaks in the PAR and CAR (Fig.3a

397 and b). Based on the *n*-alkane compositions of modern plants in this site, the lowest CPI
398 and ACL values and the highest $P_{aq}$ values (Fig.5 d-f) suggests a higher contribution of
399 *Sphagnum* spp residues that are more resistant to decomposition and commonly
400 accumulates in peat during shallow water conditions (Andersson et al., 2012; Loisel et
401 al., 2014; Zhang et al., 2016, 2018).

402 At the $YC_s$ site, the modern plants are characterized by emersed aquatic vascular
403 plants (*T. orientalis* and *P. australis*) and other aquatic plants associated with relatively
404 deeper water than at the other sites (Fig.2). Lower TOC concentrations, *n*-alkane CPI
405 and ACL values and higher $P_{aq}$ values, collectively imply a lacustrine condition with
406 smaller subaerial plant inputs before 1850 CE (Fig.6 a, d-f). Higher *n*-alkane
407 TOC-normalized concentrations in this time might have resulted from algae and bacteria
408 that are characterized by short chain *n*-alkanes (Fig.6 c-f). Higher TOC, *n*-alkane
409 concentrations, CPI and ACL values, and lower $P_{aq}$ values indicate greater inputs of
410 terrigenous vascular plants associated with continual lake infilling, promoted peat
411 accumulation from 1850 to 1900 CE (Fig.6). An evident rise in water depth occurred
412 from 1900 to 1950 CE when the aquatic plants became the major communities as
413 indicated by the highest TOC-normalized *n*-alkane concentrations, lowest *n*-alkane ACL
414 but the highest $P_{aq}$ values (Fig.6 c, e and f). Obvious decreases in both TOC and
415 TOC-normalized *n*-alkane concentrations (Fig.6 a and c) imply smaller inputs to the
416 peats from terrigenous vascular plants (Eglinton and Hamilton, 1967). However, PAR
417 reached a maximum and CAR also increased during this interval, although the
418 terrigenous vascular plant contribution to the peat was less (Fig.6b). Peat preservation

419 and accumulation are mainly controlled by the combination of the kind of OM from the
420 peat-forming plant inputs and microbial activity related to climate conditions (Zhou et
421 al., 2005, 2010; Zhang et al., 2016). The variations in peat *n*-alkane CPIs are closely
422 associated with peat-forming plants, temperature condition and microbial activity (e.g.
423 Zhou et al., 2005; Andersson and Meyers, 2012; Naafs et al., 2019). We suggest that the
424 weaker microbial activity that is indicated by relatively higher CPI values (Fig.6 d) in an
425 inferred high water-level setting from 1900 to 1950 CE was a major factor for limiting
426 peat decomposition. Since 1950 CE, the variations in TOC, PAR, TOC-normalized
427 *n*-alkane concentrations and *n*-alkane proxies reflect local conditions, and the relative
428 water level diminished to be like that in the period before 1900 CE (Fig.6).

429 Unlike $YC_w$ and $YC_s$ locations, the $YC_E$ site was dominated by terrigenous vascular
430 plants dominated by long-chain *n*-alkanes in low water depth conditions before 1800 CE
431 (Fig.7). Major inputs to the peats from large amounts of terrigenous plants started at
432 1800 CE, when obvious increases in TOC concentrations appear in the $YC_E$ location
433 (Fig.7 a). Marked changes in *n*-alkane distributions of the peat core imply variations in
434 vegetation communities in the $YC_E$ locations since 1800 CE (Fig.7 c-f); Based on the
435 *n*-alkane compositions of modern plants in this site, higher PARs and CARs from 1800
436 CE can be interpreted in terms of a greater contribution of *Sphagnum* spp. growing
437 under wetter conditions that were the major contributors of middle chain carbon lipids,
438 leading to higher *n*-alkane concentrations, elevated CPI and $P_{aq}$ values, and the lowest
439 ACL values in peat (Fig.7b-f).

440 Like the $YC_E$ location, the peat in the $YC_N$ site has clearly lower TOC

concentrations and accumulation rates during the initial time from 1750 to 1800 CE (Fig.8a and b), when fewer terrigenous vascular plants dominated by long-chain *n*-alkanes developed under drier *in situ* conditions (Fig.8d-f). Subsequently, the peat sequence received a high contribution of the middle-chain *n*-alkanes that are diagnostic of *Sphagnum* spp under inferred cold and wet conditions that stimulated peat TOC preservation and peat accumulation from 1800 to 1900 CE (e.g. Zhou et al., 2010; Andersson and Meyers, 2012; Naafs et al., 2019). After this period the *n*-alkane distributions are dominated by long chain carbon *n*-alkanes as evidenced from rapid decreases in CPI and $P_{aq}$ values and an increase in ACL values (Fig.8 d-f), providing more evidence of inputs from predominantly terrigenous vascular plant such as *Carex* and shrubs during an interval of shallow water depths since 1950 CE.

Both the plant communities that contribute to the peat deposits and the degree of preservation can be the results of different hydrological conditions (Andersson et al., 2012). Compared to other three sites, the $YC_N$ site evidently was deposited under a lower relative water level, given that the peat sequence has higher mean value of the *n*-alkane CPI (4.0 ±0.9) and ACL (27.8±1.0) but has lower $P_{aq}$ values (0.3±0.1) (Table 2), indicating that the peat originated mostly from terrigenous vascular plants. In contrast, the $YC_w$ and $YC_s$ peat cores have lower ACL (~ 25.4) but higher $P_{aq}$ (~0.7) values (Table 2), implying the prevalence of aquatic plants typified by middle-chain *n*-alkanes under deeper water depth conditions at the two sites (e.g. Cranwell et al., 1984; Ficken et al., 2000; Andersson and Meyers, 2012; Naafs et al., 2019). The initial peat deposition in the $YC_S$ site of the Yuanchi Lake was more than 200 years later than in the other three

463 sites (Fig.3). Therefore, we speculate that the Yuanchi Lake shallow basin that is
464 composed of massive volcanic lava and tephra (Yang et al., 1995) is uneven and has a
465 gradient with a higher north side and lower south and west sides. This topography
466 results in different water depths around its edges and explains the contrast between the
467 four peat sequences.

468 *4.3. Controls on local climate and peat deposition around Yuanchi Lake*

469 Because Yuanchi Lake is a closed system with no inflow or outflow (Bao et al., 2010),
470 its hydrology is mainly controlled by evaporation and precipitation. Volcanic eruptions
471 become important natural contributors to regional climate changes on many timescales,
472 and large explosive volcanism is a leading forcing agent of natural climate changes on
473 an interannual timescale (e.g. Robock, 2000; Liu et al., 2016). In general, air
474 temperatures are reduced for several years after large or high frequency eruptions,
475 because aerosols generated by volcanic eruptions could diminish solar radiation and
476 thereby impact regional and sometimes global climates (Huang et al., 2013; Liu et al.,
477 2015). *n*-Alkane-inferred climate reconstructions in the Great Hinggan Mountain,
478 northeastern China, have revealed that cold climate intervals are associated with periods
479 with a higher frequency of tropical Pacific volcanic eruptions (Mann et al., 2005; Zhang
480 et al., 2014). In the Yuanchi peatland, the initial peat deposition occurred at the $YC_W$ and
481 $YC_E$ locations around 1600 CE (Fig.3). Coincidentally, high frequency volcanic
482 activities had occurred in the tropical Pacific in this period (Mann et al., 2005) and
483 volcanic eruptions also occurred in the Changbai Mountains in 1668 and 1702 CE (Xu et
484 al., 2012). We therefore postulate that lower OM accumulations accompanied with

485 higher ash contents in the sediments before 1700 CE in these two sites record tephra
486 delivery and that cold climate conditions are consequences of the frequent volcanic
487 activities in the Pacific and the local eruptions in the Changbai Mountains (Fig. 9 f and
488 g).

489 The initial stage of transformation of lake edges into peatlands around 1800 CE
490 corresponds to a time of warmer and drier climate in northeastern China (Hong et al.,
491 2001; Lin et al., 2004; Zhang et al., 2014). Decreased volcanic activities during the
492 interval from 1700 to 1800 CE led to warmer climate conditions that stimulated more
493 terrigenous vascular plant growth and promoted peat accumulation along the shores of
494 Yuanchi Lake (Fig.9). From 1800 to 1900 CE, cool climate condition in the Yuanchi
495 region likely led to smaller OM inputs from terrigenous vascular plants as indicated by
496 relatively lower TOC-normalized total *n*-alkane concentrations (except for the YCs
497 sequence), lower CPI and ACL values, and higher $P_{aq}$ values in the peat sequences (Fig.9
498 a, c-e). Moreover, the higher ash contents deposited in the cores is likely also a local
499 response to an increase in volcanic forcing from the tropical Pacific (Fig.9f and g, Mann
500 et al., 2005) and to volcanic eruptions in the Changbai Mountains in 1898 CE and 1903
501 CE (Huang et al., 2013). Subsequently, *n*-alkane proxies in the peat cores indicate that
502 enhanced inputs of terrigenous vascular plant waxes under warm and dry climate
503 conditions around Yuanchi Lake existed from 1900 to 1950 CE and promoted peat
504 accumulation around the lake (Fig.9a-e). This multi-decadal warm/dry regional
505 transition corresponds to the period characterized by diminished volcanic activities in
506 both the Changbai Mountains and the tropical Pacific (Fig.9f).

After 1950 CE, total *n*-alkane concentrations in the four sequences drop to their minima, and obvious decreases in PAR values occurred in the high-water level locations (the $YC_W$ and $YC_S$ sites) (Fig.9a-b). These *n*-alkane proxies imply that the Yuanchi region experienced a significantly cooler climate accompanied with decreased terrigenous vascular plant inputs in recent years, as reflected in the higher CPI, lower ACL, and higher $P_{aq}$ values in the peat sequences (Fig. 9c-e). This multidecadal period of cold climate might be attributed to a series of volcanic activities in the tropical Pacific (Fig.9f) that released abundant aerosols and thereby diminished solar radiation (Robock, 2000; Huang et al., 2013; Liu et al., 2016). In addition, the beginning of the Anthropocene in the Changbai Mountain region could be defined as 1950 CE due to the rapid industrial and urban development after the Reform and Opening-Up of China (Bao et al., 2019). As part of this development, greater combustion of fossil fuels and biomass from expanding anthropogenic sources led to increases in their soot emissions and more black carbon being deposited in peat (Gao et al., 2016). Substantial increases since 1950 CE in Pb accumulation rates in the Yuanchi peat further indicate significant deterioration of the mountain environment from magnifying human impacts (Fig.9g). Therefore, we postulate that anthropogenic impacts on the mountain region since 1950 CE likely suppressed growth of land plants, reduced OM inputs from subaerial vascular plants, and slowed peat accumulation.

## 5. Conclusion

*n*-Alkane biomarkers from the four peat cores around Yuanchi Lake in the Changbai Mountains, northeastern China, record peat depositional processes in a typical maar lake

on a decadal scale. Although different lengths of peat sequences were collected around Yuanchi Lake, the initiation for abundant peat accumulation (ca. 1800 CE) at the four locations was similar. Based on *n*-alkane compositions in modern plants at the four sites, *n*-alkane distributions in the four peat cores indicate that different vegetation communities under different hydrological conditions contributed to differences in peat accumulation rates and compositions of the four peat sequences. We postulate that the differences in peat deposition between the four sites is a consequence of different peat-forming communities growing in different water depths that are the results of the uneven basement rock topography of the lake basin caused by volcanogenic origin from lava and tephra.

*n*-Alkane-inferred regional climate changes have impacted peat accumulations, but in ways that are shared by the four locations. Lower peat accumulation rates record diminished OM inputs from terrigenous vascular plant during two long-term intervals from 1600 to 1700 CE and 1800 to 1900 CE, which both correspond to cooler climate associated with high-frequency volcanic eruptions in the tropical Pacific and in the Changbai Mountains. A lower rate of volcanic eruptions contributed to warm/dry regional conditions from 1700 to 1800 CE and 1900 to 1950 CE, when large terrigenous vascular plant input and promoted peat accumulation. Since 1950 CE, lower peat accumulation rates with diminished OM inputs from terrigenous vascular plants have existed during a significantly cooler climate in the Yuanchi region that coincides with both a series of volcanic eruptions and anthropogenic activities.

## Data Availability Statement

551 Analytical data are available from Deep Blue Data ( ) and from the cited
552 references.

553 **Acknowledgments**

554 We thank the Analysis and Test Center of the Northeast Institute of Geography and
555 Agroecology, Chinese Academy of Sciences, for sample analysis. The study was
556 supported by funds from the Natural Science Foundation of China (no.41807439) and
557 the Natural Science Foundation of Fujian Province, China (no.2019J05067).

558 **Author Contributions**

559 YZ, CG, SZ, PY, and GW conceived and designed the study. YZ, CG, SZ, and PY
560 facilitated and conducted the field work. YZ did the lab analyses and analyzed the data.
561 YZ and PAM wrote the paper. All authors contributed to the drafts of the paper and its
562 final approval.
563

8

**References:**


Andersson, R.A, Kuhry, P., Meyers, P., Zebühr, Y., Crill, P., & Mörth, M. (2011). Impacts of paleohydrological changes on *n*-alkane biomarker compositions of a Holocene peat sequence in the eastern European Russian Arctic. *Organic Geochemistry*, 42, 1065-1075. https://doi.org/10.1016/j.orggeochem.2011.06.020

Andersson, R. A., Meyers, P., Hornibrook, E., Kuhry, P., & Mörth, C. M. (2012). Elemental and isotopic carbon and nitrogen records of organic matter accumulation in a Holocene permafrost peat sequence in the East European Russian Arctic. *Journal of Quaternary Science*, 27, 545-552. https://doi.org/10.1002/jqs.2541

Bao, K., Yu, X.F., Jia, L., & Wang G.P. (2010). Recent Carbon Accumulation in Changbai Mountain Peatlands, Northeast China. *Mountain Research & Development*, 30, 33-41. http://dx.doi.org/10.1659/MRD-JOURNAL-D-09-00054.1

Bao, K., Wang G.P., Jia, L., & Xing, W. (2019). Anthropogenic impacts in the Changbai Mountain region of NE China over the last 150 years: geochemical records of peat and altitude effects. *Environmental Science and Pollution Research*, 26, 7512-7525. https://doi.org/10.1007/s11356-019-04138-w

Bass, M., Pancost, R., van Geel, B., & Sinninghe-Damste, J. (2000). A comparative study of lipids in *Sphagnum* species. *Organic Geochemistry*, 31, 535-541. https://doi.org/ 10.1016/S0146-6380(00)00037-1

Bingham, E.M., McClymont, E.L., & Väliranta, M. (2010) . Conservative composition of *n*-alkane biomarkers in *Sphagnum* species: Implications for palaeoclimate

586 reconstruction in ombrotrophic peat bogs. *Organic Geochemistry*, 41, 214-220.
587 https://doi.org/10.1016/j.orggeochem.2009.06.010
588 Chai, X. (1990). Peat-geology. Geological Publishing House, Beijing, pp. 136-309 (in
589 Chinese).
590 Cranwell, P.A. (1984). Lipid geochemistry of sediments from Upton Broad, a small
591 productive lake. *Organic Geochemistry*, 7, 25-37.
592 https://doi.org/10.1016/0146-6380(84)90134-7
593 Eglinton, G., & Hamilton, R.J. (1967). Leaf epicuticular waxes. Science, 156 (3780),
594 1322-1335. https://doi.org/10.1126/science.156.3780.1322
595 Ficken, K.J, Li, B., Swain, D.L., & Eglinton, G. (2000). An *n*-alkane proxy for the
596 sedimentary input of submerged/floating freshwater aquatic macrophytes. *Organic*
597 *Geochemistry*, 31, 745-749. https://doi.org/10.1016/S0146-6380(00)00081-4
598 Gao, C., Knorr, K.H., Yu, Z., He, J., Zhang, S., Lu, X., et al. (2016). Black carbon
599 deposition and storage in peat soils of the Changbai Mountain, China. *Geoderma*,
600 273, 98-105. http://dx.doi.org/10.1016/j.geoderma.2016.03.021
601 Hong, Y.T., Wang, Z.G., Jiang, H.B., Lin, Q.H., Hong, B., Zhu, Y.X., et al. (2001). A
602 6000-year record of changes in drought and precipitation in northeastern China
603 based on a $\delta^{13}C$ time series from peat cellulose. *Earth and Planetary Science Letters*,
604 185, 111-119. https://doi.org/10.1016/S0012-821X(00)00367-8
605 Huang, T. (2013). Peatland archives of Holocene volcanic eruption response to
606 paleoclimate in Northeast China (Doctoral Thesis). China University of Geosciences,
607 Wuhan, China. (In Chinese)

608 Kayranli, B., Scholz, M., Mustafa, A., & Hedmark, Å. (2010). Carbon storage and fluxes
609 within freshwater wetlands: a critical review. *Wetlands*, 30, 111-124.
610 https://doi.org/10.1007/s13157-009-0003-4
611 Lin, Q.H., Leng, X.T., & Hong, B. (2004). The Peat Record of 1ka of Climate Change in
612 Daxing Anling. Bulletin of Mineralogy, *Petrology and Geochemistry*, 23, 15-18 (In
613 Chinese).
614 Liu, F., Chai, J., Wang, B., Liu, J., Zhang, X., & Wang, Z.Y. (2016). Global monsoon
615 precipitation responses to large volcanic eruptions. *Scientific Reports*, 6,
616 https://doi.org/10.1038/srep24331
617 Mann, M.E., Cane, M.A., Zebiak, S.E., & Clement, A. (2005). Volcanic and Solar
618 Forcing of the Tropical Pacific over the past 1000 years. *Journal of climate*, 18, 447-
619 456.
620 Naafs, B.D.A., Inglis, G.N., Blewett, J., McClymont, E.L., Lauretano,V., Xie, S., et al.
621 (2019). The potential of biomarker proxies to trace climate, vegetation, and
622 biogeochemical processes in peat: A review. *Global and Planetary Change*, 179,
623 57-79. https://doi.org/10.1016/j.gloplacha.2019.05.006
624 Nichols, J.E., Booth, R.K., Jackson, S.T., Pendall, E.G., & Huang, Y.S. (2006).
625 Paleohydrologic reconstruction based on *n*-alkane distributions in ombrotrophic peat.
626 *Organic Geochemistry*, 37, 1505-1513. https://doi.org/10.1016/j. orggeochem. 2006.
627 06. 020
628 Regnery, J., Püttman, W., Koutsodendris, A., Mulch, A., & Pröss, J. (2013). Comparison
629 of paleoclimatic significance of higher land plant biomarker concentrations and

630 pollen data: A case study of lake sediments from the Holsteinian interglacial. *Organic*
631 *Geochemistry*, 61, 73-84. https://doi.org/10.1016/j.orggeochem.2013.06.006
632 Robock, A. (2000). Volcanic Eruptions and Climate. *Reviews of Geophysics*, 38,
633 191-219. https://doi.org/10.1029/1998RG000054
634 Ronkainen, T., McClymont, E.L., Valiranta, M., & Tuittila, E.S. (2013). The *n*-alkane
635 and
636 sterol composition of living fen plants as a potential tool for palaeoecological studies.
637 *Organic Geochemistry*, 59, 1-9. https://doi.org/10.1016/j.orggeochem.2013.03.005
638 Salasoo, I. (1987). Alkane distribution in epicuticular wax of some heath plants in
639 Norway. *Biochemical Systematics and Ecology*, 15, 663-665.
640 https://doi.org/10.1016/0305-1978(87)90041-X
641 Seki, O., Meyers, P.A., Kawamura, K., Zheng, Y., & Zhou, W. (2009). Hydrogen
642 isotopic
643 ratios of plant-wax n-alkanes deposited in a peat bog in northeastern China during the
644 last 16 ky. *Organic Geochemistry*, 40, 671-677. https://doi.org /10.1016
645 /j.orggeochem. 2009.03.007
646 Street, J.H., Anderson, R.S., Rosenbauer, R.J., & Paytan, A. (2012). *n*-Alkane evidence
647 for the onset of wetter conditions in the Sierra Nevada, California (USA) at the
648 mid-late Holocene transition ~ 3.0 ka. *Quaternary Research*, 79, 14-23.
649 https://doi.org /10.1016/j.yqres.2012.09.004
650 Sun, C.Q., Plunkett, G., Liu, J., Zhao, H., Sigl, M., McConnell, J.R., et al. (2014). Ash
651 from Changbaishan Millennium Eruption recorded in Greenland ice: Implications for

652 determining the eruption's timing and impact. *Geophysical Research Letters*, 41,
653 694-701. https://doi.org/10.1002/2013GL058642
654 Sun, C. Q., You, H.T., He, H.Y., Zhang, L., Gao, J.L., Guo, W.F., et al. (2015). New
655 evidence for the presence of Changbaishan Millennium Eruption ash in the Longgang
656 volcanic field, Northeast China. *Gondwana Research*, 28, 52-60. http://dx. doi.org/
657 10.1016/j.gr.2015.01.013
658 Tarasov, P.E., Müller, S., Zech, M., Andreeva, D., Diekmann, B., & Leipe, C. (2013).
659 Last glacial vegetation reconstructions in the extreme-continental eastern Asia:
660 Potentials of pollen and *n*-alkane biomarker analyses. *Quaternary International*, 290,
661 253- 263. https://doi.org/10.1016/j.quaint.2012.04.007
662 Xing, W., Bao, K.S., Han, D.X., & Wang, G.P. (2019). Holocene wetland developing
663 history and its response to climate change in northeast China. *Journal of Lake*
664 *Sciences*, 31(5), 1391-1402. (In Chinese)
665 Xu, J., Liu, G., Wu, J., Ming, Y., Wang, Q., Cui, D., et al. (2012). Recent unrest of
666 Changbaishan volcano, northeast China: A precursor of a future eruption?
667 *Geophysical Research Letters*, 39, 1-7. https://doi.org/10.1029/2012GL052600
668 Yang, Y.X. (1995). Study on the formation and development of mire and
669 paleoenvironment changes since the Holocene in the Northeast region (Doctoral
670 Thesis). Changchun Institute of Geography, the Chinese Academy of Sciences,
671 Changchun, China. (In Chinese)
672 Zhang, Y., Liu, X.T., Lin, Q.X., Gao, C.Y., Wang, J. & Wang, G.P. (2014). Vegetation
673 and climate change over the past 800 years in the monsoon margin of northeastern

China reconstructed from *n*-alkanes from the Great Hinggan Mountain ombrotrophic peat bog. *Organic Geochemistry*, 76, 128-135. http://dx.doi.org/10.1016/j.orggeochem.2014.07.013

Zhang, Y., Meyers, P.A., Liu, X.T., Wang, G.P., Ma, X.H., Li, X.Y., et al. (2016). Holocene climate changes in the central Asia mountain region inferred from a peat sequence from Altai Mountains, Xinjiang, northwestern China. *Quaternary Science Reviews*, 152, 19-30. http://dx.doi.org/10.1016/j.quascirev.2016.09.016

Zhang, Y., Yang, P., Tong, C., Liu, X., Zhang, Z., Wang, G., et al. (2018). Palynological record of Holocene vegetation and climate changes in a high-resolution peat profile from the Xinjiang Altai Mountains, northwestern China. *Quaternary Science Reviews*, 201, 111-123. https://doi.org/10.1016/j.quascirev.2018.10.021

Zheng, Y.H., Zhou, W.J., Meyers, P.A., & Xie, S.C. (2007). Lipid biomarkers in the Zoigê-Hongyuan peat deposit: Indicators of Holocene climate changes in West China. *Organic Geochemistry*, 38, 1927-1940. https://doi.org/10.1016/j.orggeochem. 2007.06.012

Zhou, W.J., Xie, S.C., Meyers, P.A., & Zheng, Y.H. (2005). Reconstruction of late glacial and Holocene climate evolution in southern China from geolipids and pollen in the Dingan peat sequence. *Organic Geochemistry*, 36, 1272-1284. https://doi.org/10.1016/j.orggeochem.2005.04.005

Zhou, W., Zheng, Y., Meyers, P. A., Jull, A. J. T. & Xie, S. (2010). Postglacial climate-change record in biomarker lipid compositions of the Hani peat sequence,

695 northeastern China. *Earth and Planetary Science Letters*, 294, 37-46. https://doi.org/
696 10.1016/ j.epsl.2010.02.035
697

## Figure legends

**Fig. 1.** Location of the sampling site from the Yuanchi peatland in the Changbai Mountains, northeastern China.

**Fig. 2.** Panoramic views of Yuanchi Lake and of the four different sampling sites (west, south, east and north) in the peatlands surrounding the lake. (Photos by Guoping Wang)

**Fig.3.** Lithostratigraphy, $^{210}$Pb-inferred age-depth model (a, c, e and g), the TOC concentrations (black lines, Bao et al., 2010) and peat accumulation rates (PAR, red lines) (b, d, f and h) of the four peat cores from the west, south, east, and north sides ($YC_W$, $YC_S$, $YC_E$, $YC_N$, respectively) around Yuanchi Lake.

**Fig.4.** Distributions relative to the major *n*-alkane in samples from different depths of the four peat cores around Yuanchi Lake.

**Fig.5.** Downcore variations of TOC concentrations (a), carbon accumulation rates (CAR) (b, black line) and PAR values (red line), Total *n*-alkane concentrations relative to TOC (c), *n*-alkane CPI (d), ACL (e) and $P_{aq}$ (f) values from the western site of the Yuanchi peatland ($YC_w$). TOC and CAR values from Bao et al., 2010. The red dotted lines represent the intervals characterized by different variations in those proxies.

**Fig.6.** Downcore variations of TOC concentrations (a), carbon accumulation rates (CAR) (b, black line) and PAR values (red line), Total *n*-alkane concentrations relative to TOC (c), *n*-alkane CPI (d), ACL (e) and $P_{aq}$ (f) values from the southern site of the Yuanchi peatland ($YC_S$). TOC and CAR values from Bao et al., 2010. The

720 red dotted lines represent the intervals characterized by different variations in those
721 proxies.

722 **Fig.7.** Downcore variations of TOC concentrations (a), carbon accumulation rates
723 (CAR) (b, black line) and PAR values (red line), Total *n*-alkane concentrations
724 relative to TOC (c), *n*-alkane CPI (d), ACL (e) and $P_{aq}$ (f) values from the eastern site
725 of the Yuanchi peatland ($YC_E$). TOC and CAR values from Bao et al., 2010. The red
726 dotted lines represent the intervals characterized by different variations in those
727 proxies.

728 **Fig.8.** Downcore variations of TOC concentrations (a), carbon accumulation rates
729 (CAR) (b, black line) and PAR values (red line), Total *n*-alkane concentrations
730 relative to TOC (c), *n*-alkane CPI (d), ACL (e) and $P_{aq}$ (f) values from the northern
731 site of the Yuanchi peatland ($YC_N$) over the past 150 years. TOC and CAR values
732 from Bao et al., 2010. The red dotted lines represent the intervals characterized by
733 different variations in those proxies.

734 **Fig.9.**The colored dotted lines represent total *n*-alkane concentrations relative to TOC
735 contents (a), PAR (b), *n*-alkane CPI (c), ACL (d), $P_{aq}$ values (e) and ash contents (f,
736 ASH%, Bao et al., 2010) of the four sites peat cores, respectively; Red dotted lines in
737 (a-f) represent of those proxies in $YC_W$ peat core; blue dotted lines represent of YCs
738 peat core; black dotted lines represent of $YC_E$ peat core; green dotted lines represent
739 of $YC_N$ peat core. Volcanic forcing of the tropical Pacific from a model of the tropical
740 Pacific coupled ocean-atmosphere system studied by Mann et al. (2005) (g); Red solid
741 line in (g) represents Pb accumulation rate (Pb AR) in the peat core from Yuanchi

peatland studied by Bao et al., 2019. The gray shaded areas represent the intervals characterized by cold local conditions associated with high volcanic forcing of the tropical Pacific and anthropogenic activities in the Changbai Mountains region.

**Table1**.
Major modern plant species around Yuanchi Lake in Changbai Mountains with dominant *n*-alkane homologues in those plants.

| Major modern species | | Major homologue associated to plant |
|---|---|---|
| Trees | Larix olgensis | $C_{27}$, $C_{29}$ [a] |
| | *Betula fruticosa* | $C_{27}$ [a] |
| Shrubs | *Vaccinium uliginosum* | $C_{29}$ [a] |
| | *Rhododendron parvifolium* | $C_{29}$, $C_{31}$ [a,b] |
| | *Ledum palustre L.* | $C_{29}$, $C_{31}$ [a,c] |
| Sedges | *Carex lasiocarpa* | $C_{29}$ [d] |
| | *Scirpus triqueter* | $C_{29}$, $C_{31}$ [b] |
| | *Eriophorum fauriei* | $C_{27}$ [a] |
| | *Equisetum hiemale* | $C_{29}$ [e] |
| Mosses | *Sphagnum* spp | $C_{23}$, $C_{25}$ [d,f,g,h] |
| Emergent macrophytes | *Typha orientalis* | $C_{29}$ [i,j] |
| | *Phragmites australis* | |
| Aquatic plants | Submerged and foating plants | $C_{21}$, $C_{23}$ and $C_{25}$ [i,j] |

[a] Tarasov et al. (2013); [b] Street et al. (2013); [c] Salasoo (1987); [d] Ronkainen et al. (2013); [e]Andersson et al. (2011); [f] Bass et al., 2000; [g] Nichols et al., 2006; [h] Bingham et al., 2010; [i] Cranwell et al. (1984); [j]Ficken et al. (2000);

**Figure.**

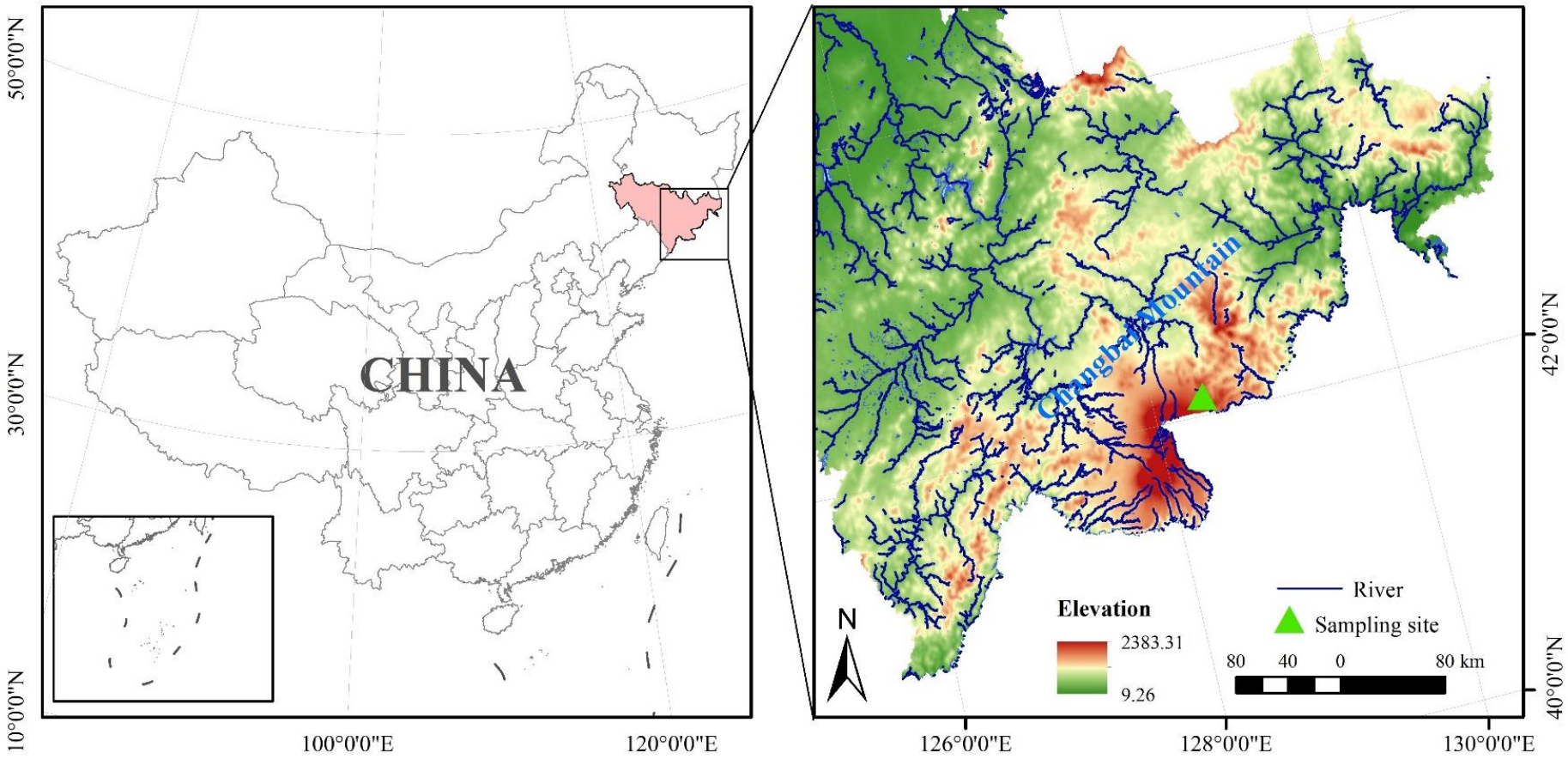
CHINA
50°0'0"N
30°0'0"N
10°0'0"N
100°0'0"E
120°0'0"E
Changbai Mountain
N
Elevation
2383.31
9.26
River
Sampling site
80 40 0 80 km
42°0'0"N
40°0'0"N
126°0'0"E
128°0'0"E
130°0'0"E

**Figure.**


E
N
E
N
S
W
W
S

**Figure.**

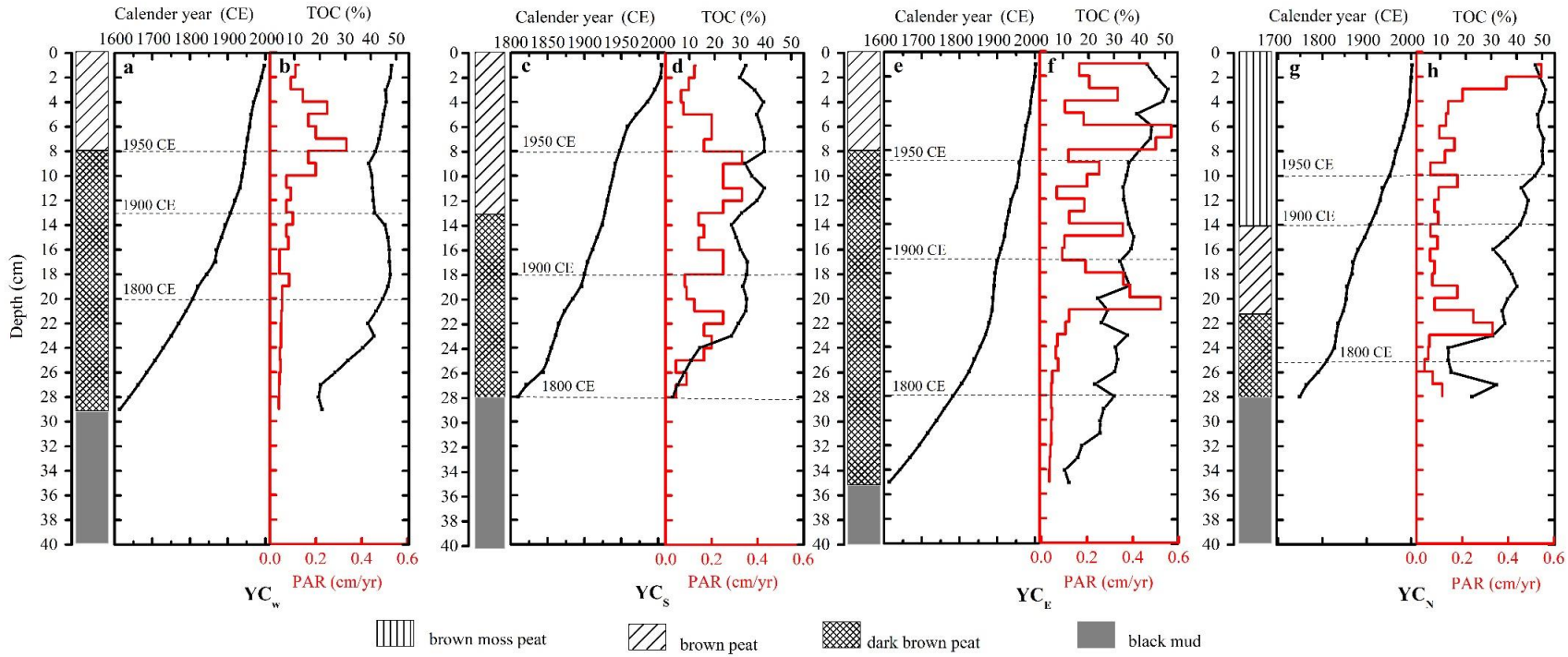
Calender year (CE)
TOC (%)
Depth (cm)
a
b
c
d
e
f
g
h
1950 CE
1900 CE
1800 CE
PAR (cm/yr)
YC_w
YC_S
YC_E
YC_N
brown moss peat
brown peat
dark brown peat
black mud

**Figure.**

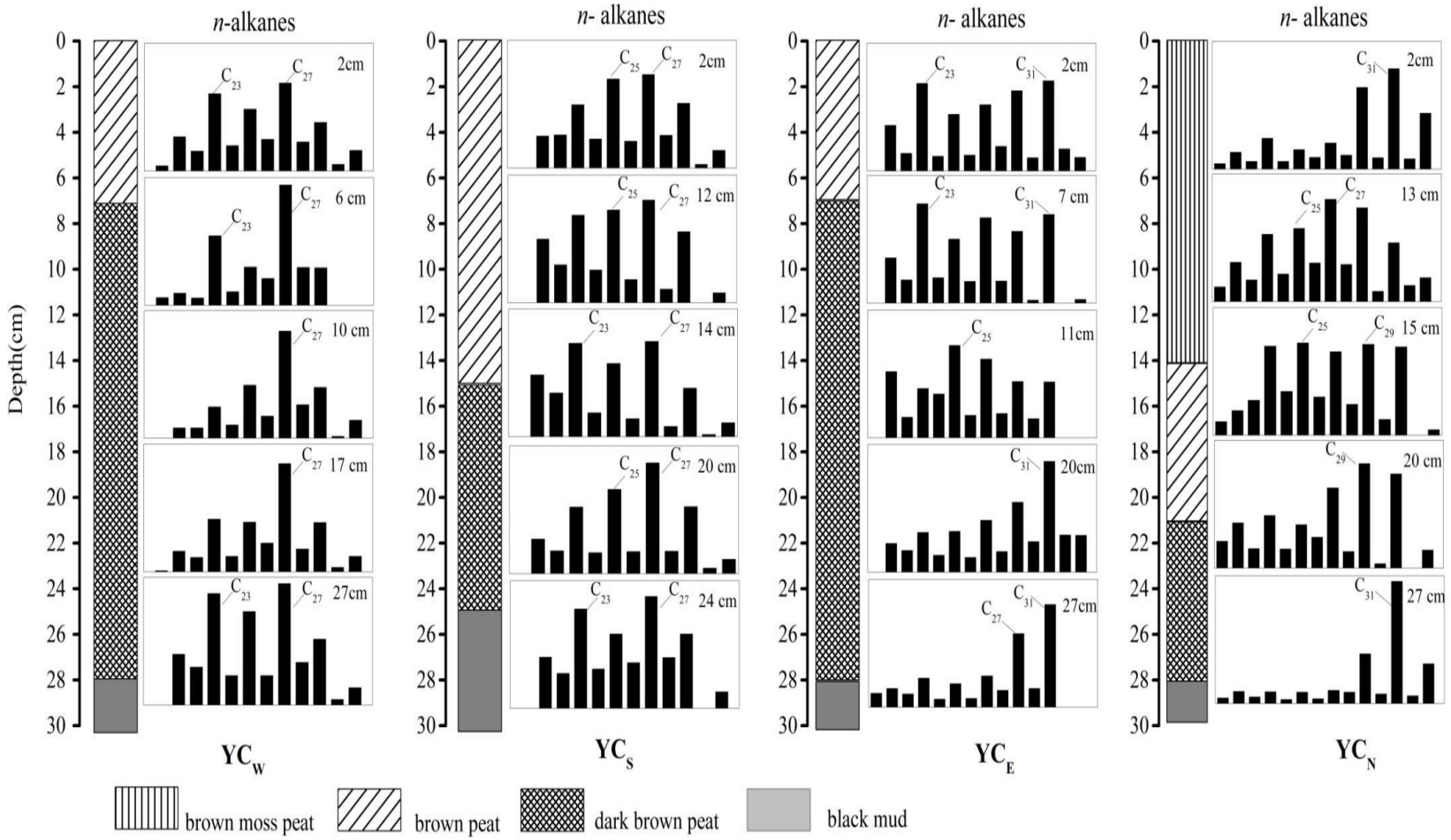
n-alkanes
n- alkanes
n- alkanes
n- alkanes
Depth(cm)
0
2
4
6
8
10
12
14
16
18
20
22
24
26
28
30
C23
C27
2cm
6 cm
10 cm
17 cm
27cm
C25
12 cm
14 cm
20 cm
24 cm
C31
7 cm
11cm
20cm
27cm
C29
13 cm
15 cm
20 cm
27 cm
YCW
YCS
YCE
YCN
brown moss peat
brown peat
dark brown peat
black mud

**Figure.**

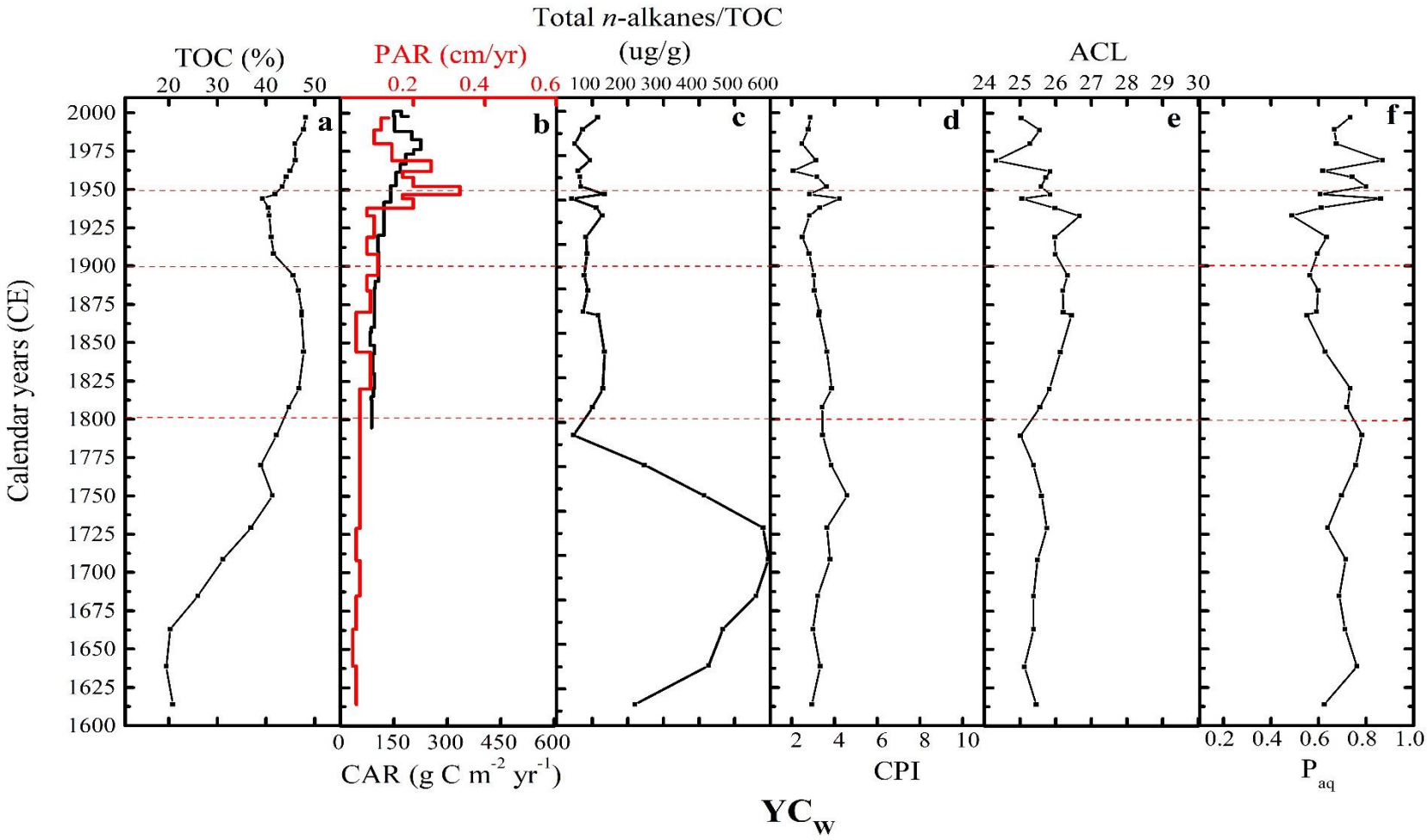
Total n-alkanes/TOC
(ug/g)
TOC (%)
PAR (cm/yr)
ACL
a
b
c
d
e
f
Calendar years (CE)
2000
1975
1950
1925
1900
1875
1850
1825
1800
1775
1750
1725
1700
1675
1650
1625
1600
20 30 40 50
0.2 0.4 0.6
100 200 300 400 500 600
24 25 26 27 28 29 30
0 150 300 450 600
CAR (g C m-2 yr-1)
2 4 6 8 10
CPI
0.2 0.4 0.6 0.8 1.0
Paq
YCw

**Figure.**

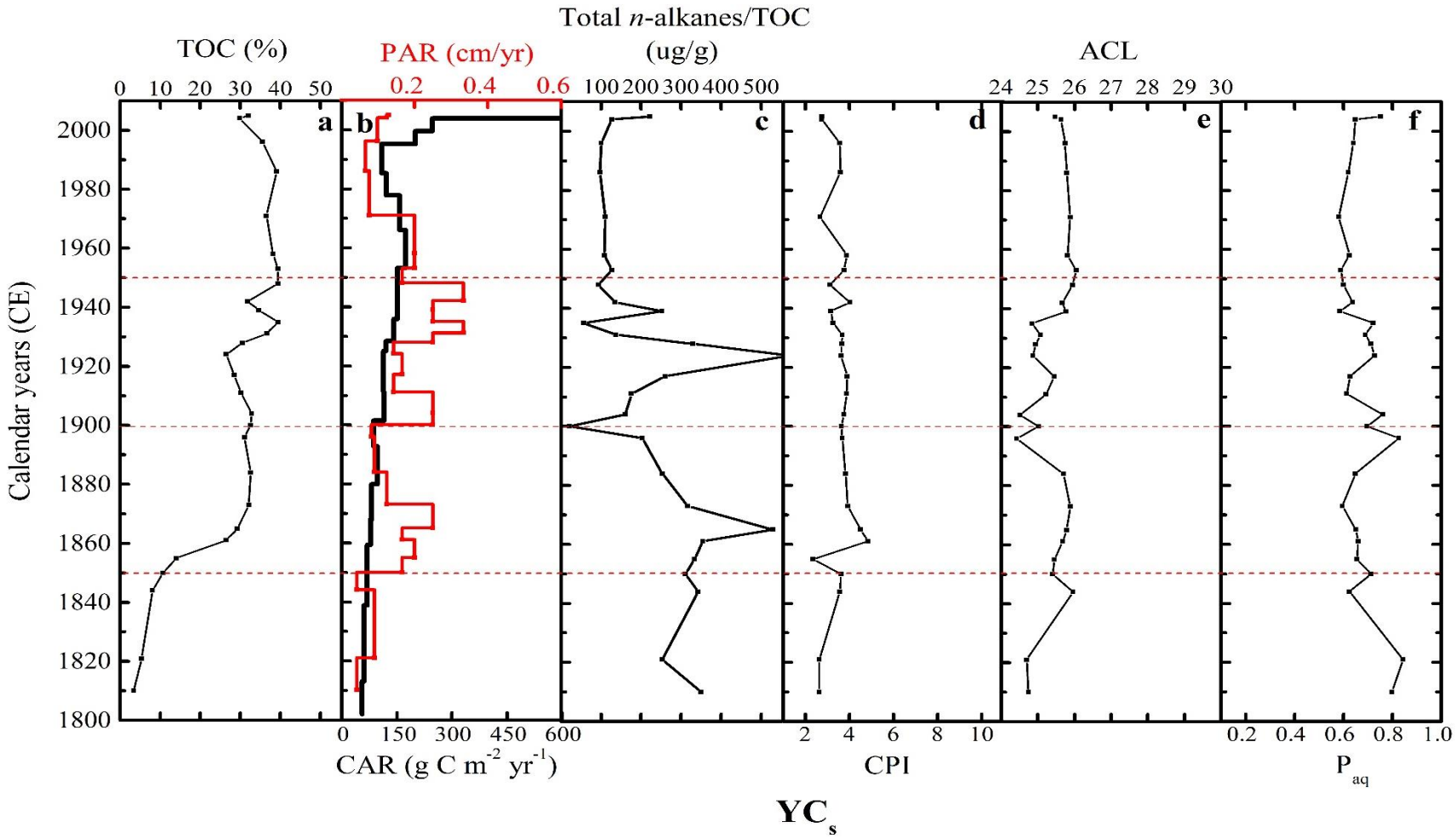
Total *n*-alkanes/TOC
TOC (%)
PAR (cm/yr)
(ug/g)
ACL
0 10 20 30 40 50
0.2 0.4 0.6
100 200 300 400 500
24 25 26 27 28 29 30
a
b
c
d
e
f
Calendar years (CE)
2000
1980
1960
1940
1920
1900
1880
1860
1840
1820
1800
0 150 300 450 600
CAR (g C m$^{-2}$ yr$^{-1}$)
2 4 6 8 10
CPI
0.2 0.4 0.6 0.8 1.0
$P_{aq}$
**$YC_s$**

**Figure.**

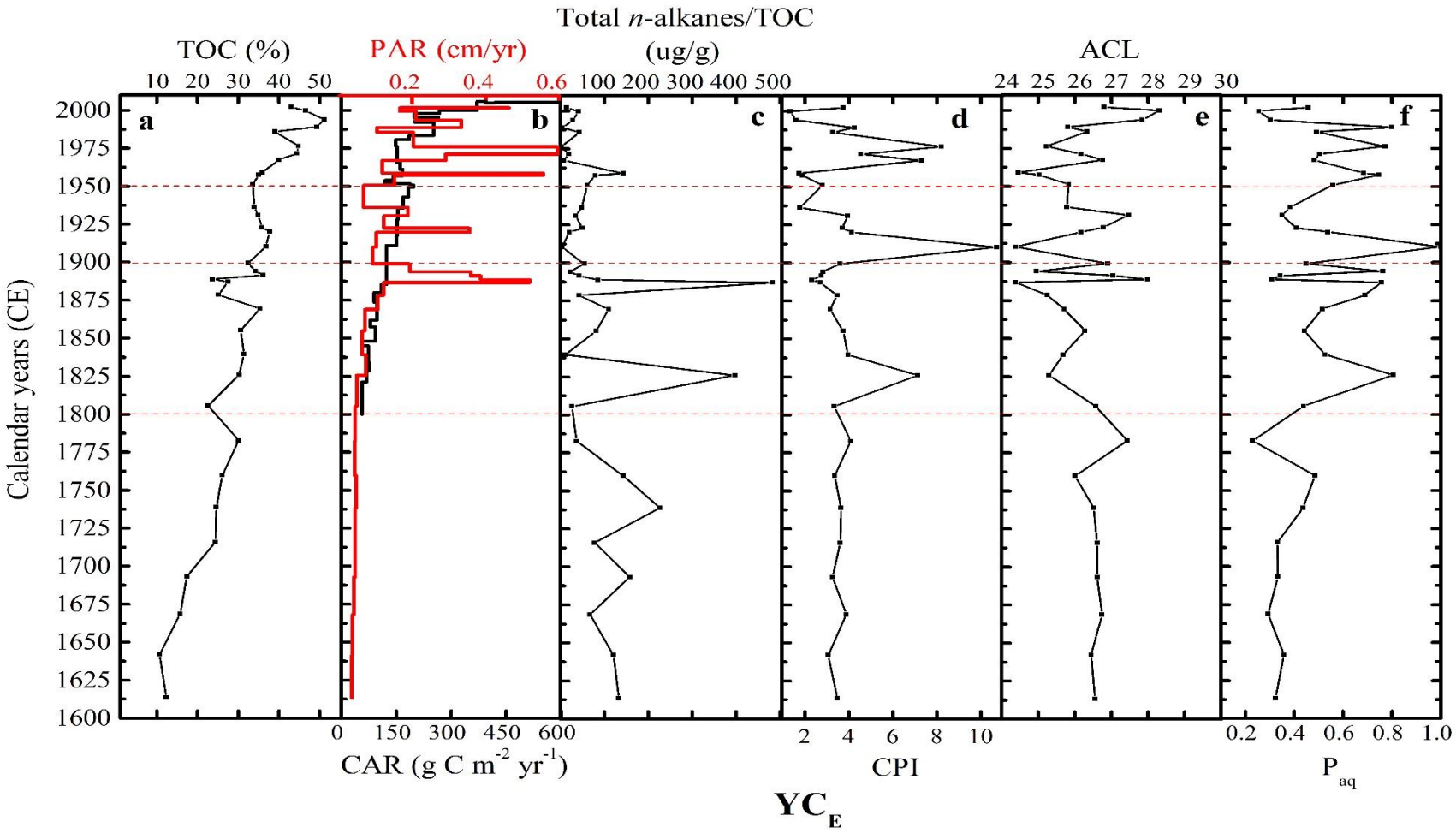
Total *n*-alkanes/TOC
TOC (%)
PAR (cm/yr)
(ug/g)
ACL
10 20 30 40 50
0.2 0.4 0.6
100 200 300 400 500
24 25 26 27 28 29 30
a
b
c
d
e
f
Calendar years (CE)
2000
1975
1950
1925
1900
1875
1850
1825
1800
1775
1750
1725
1700
1675
1650
1625
1600
0 150 300 450 600
CAR (g C m$^{-2}$ yr$^{-1}$)
2 4 6 8 10
CPI
0.2 0.4 0.6 0.8 1.0
$P_{aq}$
$YC_E$

**Figure.**

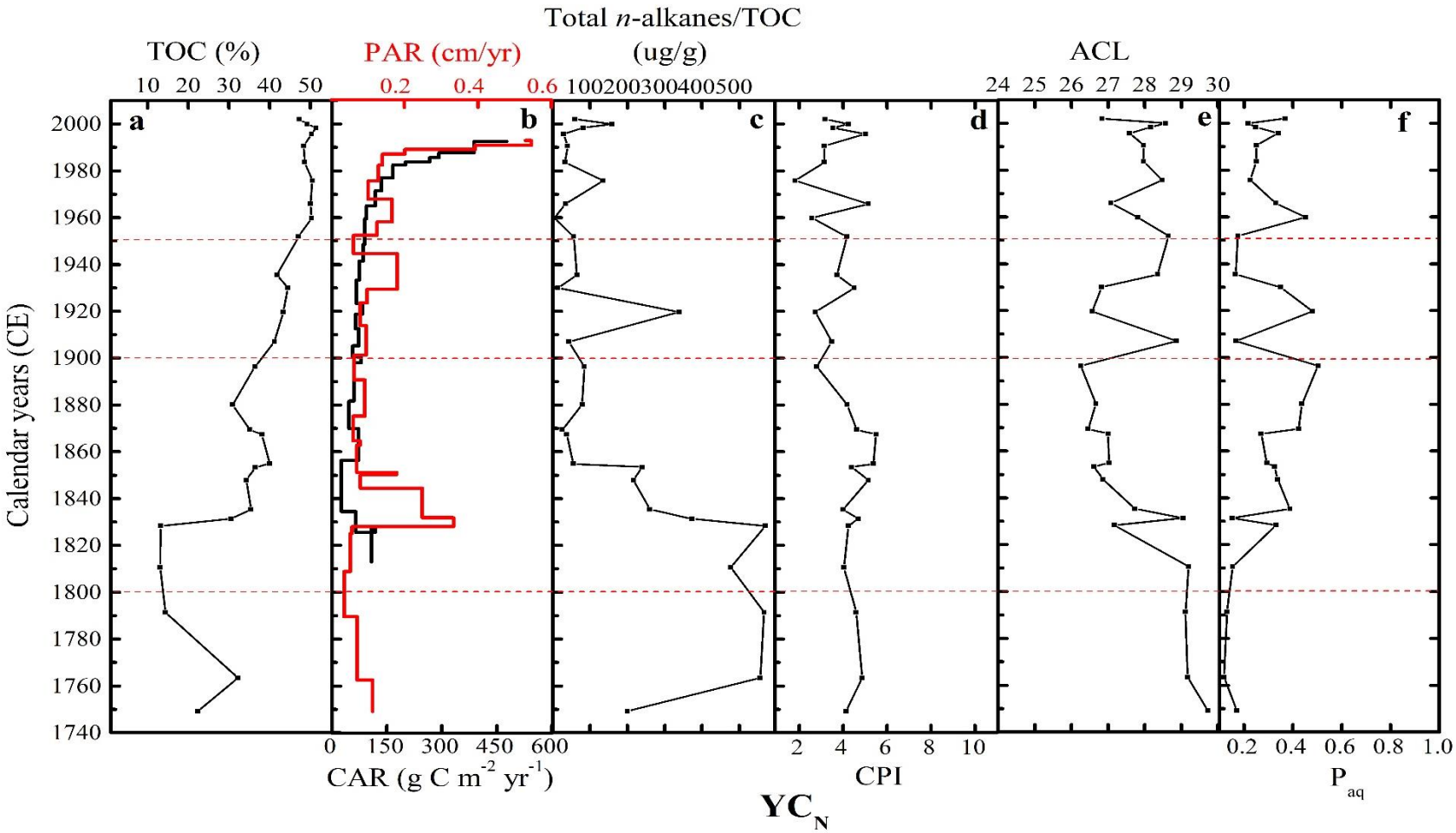
Total n-alkanes/TOC
TOC (%)
PAR (cm/yr)
(ug/g)
ACL
10 20 30 40 50
0.2 0.4 0.6
100200300400500
24 25 26 27 28 29 30
a
b
c
d
e
f
Calendar years (CE)
2000
1980
1960
1940
1920
1900
1880
1860
1840
1820
1800
1780
1760
1740
0 150 300 450 600
CAR (g C m-2 yr-1)
2 4 6 8 10
CPI
0.2 0.4 0.6 0.8 1.0
Paq
YCN

**Figure.**

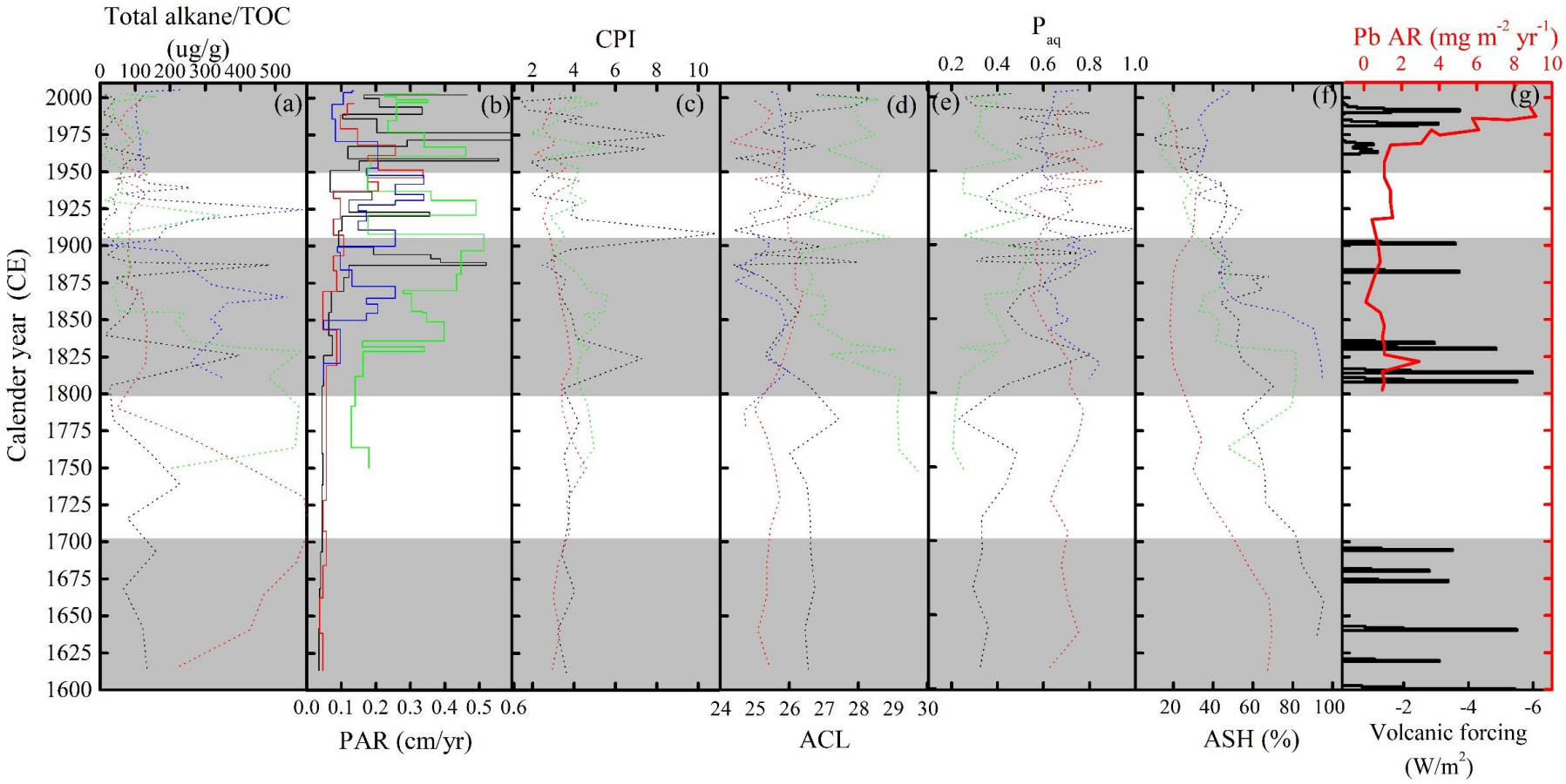
Total alkane/TOC
(ug/g)
0 100 200 300 400 500
CPI
2 4 6 8 10
P aq
0.2 0.4 0.6 0.8 1.0
Pb AR (mg m-2 yr-1)
0 2 4 6 8 10
(a)
(b)
(c)
(d)
(e)
(f)
(g)
Calender year (CE)
2000
1975
1950
1925
1900
1875
1850
1825
1800
1775
1750
1725
1700
1675
1650
1625
1600
0.0 0.1 0.2 0.3 0.4 0.5 0.6
PAR (cm/yr)
24 25 26 27 28 29 30
ACL
20 40 60 80 100
ASH (%)
-2 -4 -6
Volcanic forcing
(W/m2)